Acta Crystallographica Section D
Biological Crystallography
ISSN 0907-4449

Structural characterization of tartrate dehydrogenase: a versatile enzyme catalyzing multiple reactions

Radhika Malik‡ and Ronald E. Viola*

Department of Chemistry, University of Toledo, Toledo, Ohio 43606, USA

‡ Current address: Mount Sinai School of Medicine, Department of Structural and Chemical Biology, New York, NY 10029, USA.

Correspondence e-mail: ron.viola@utoledo.edu

Received 14 December 2009
Accepted 8 March 2010

PDB Reference: tartrate dehydrogenase, 3flk.

The first structure of an NAD-dependent tartrate dehydrogenase (TDH) has been solved to 2 Å resolution by single anomalous diffraction (SAD) phasing as a complex with the intermediate analog oxalate, Mg^{2+} and NADH. This TDH structure from *Pseudomonas putida* has a similar overall fold and domain organization to other structurally characterized members of the hydroxy-acid dehydrogenase family. However, there are considerable differences between TDH and these functionally related enzymes in the regions connecting the core secondary structure and in the relative positioning of important loops and helices. The active site in these complexes is highly ordered, allowing the identification of the substrate-binding and cofactor-binding groups and the ligands to the metal ions. Residues from the adjacent subunit are involved in both the substrate and divalent metal ion binding sites, establishing a dimer as the functional unit and providing structural support for an alternating-site reaction mechanism. The divalent metal ion plays a prominent role in substrate binding and orientation, together with several active-site arginines. Functional groups from both subunits form the cofactor-binding site and the ammonium ion aids in the orientation of the nicotinamide ring of the cofactor. A lysyl amino group (Lys192) is the base responsible for the water-mediated proton abstraction from the C2 hydroxyl group of the substrate that begins the catalytic reaction, followed by hydride transfer to NAD. A tyrosyl hydroxyl group (Tyr141) functions as a general acid to protonate the enolate intermediate. Each substrate undergoes the initial hydride transfer, but differences in substrate orientation are proposed to account for the different reactions catalyzed by TDH.

1. Introduction

Tartrate dehydrogenase (TDH) is an unusual NAD-dependent enzyme that exhibits a multiplicity of catalytic activities at a single active site (Tipton & Peisach, 1990). These activities arise from the capacity of this enzyme to catalyze a reaction pathway in which different substrates undergo the same initial catalytic steps but the subsequent intermediates can dissociate from the enzyme at different stages in the catalytic cycle, thereby leading to different final products (Tipton, 1996). β-Hydroxy-acid dehydrogenases such as TDH generally produce a β-keto acid that may either be released from the enzyme or retained and subsequently decarboxylated. TDH is unique compared with other hydroxy-acid dehydrogenases in that the decarboxylation step which it catalyzes depends on the structure and stereochemistry of the respective substrates (Ruszczycky & Anderson, 2004).

TDH is found in a variety of microorganisms and functions as part of a pathway through which tartrate is converted into

D-glycerate, thereby providing entry of these C atoms into primary metabolic pathways (Tipton, 2000). TDH from *Pseudomonas putida* has close sequence homology to prokaryotic isopropylmalate dehydrogenases (IPMDHs; ~35% identity) and to yeast homoisocitrate dehydrogenase (HIcDH; 34% identity) and to a lesser extent to *Escherichia coli* isocitrate dehydrogenase (ICDH; 25% identity) (Fig. 1). Interestingly, sequence-homology differences within the hydroxy-acid dehydrogenase family allow further classification based on the stereochemistry of the substrates and also on whether the enzyme can catalyze the subsequent decarboxylation of the reaction intermediate. Thus, (*S*)-hydroxy-acid dehydrogenases show little homology to (*R*)-hydroxy-acid dehydrogenases and are also quite distinct from the metal-

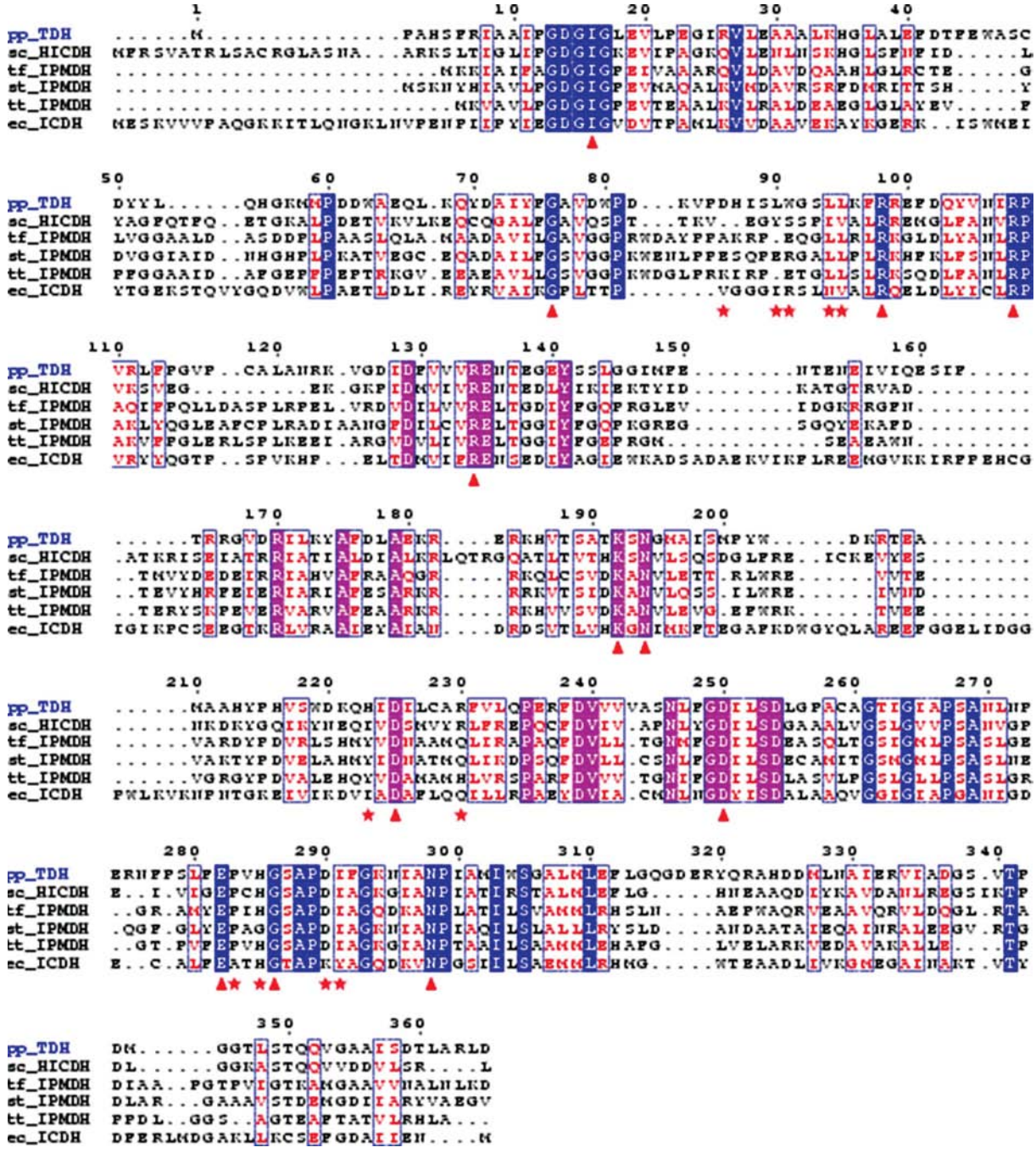

Figure 1
Sequence alignment of *P. putida* TDH (pp_TDH) with representative hydroxy-acid dehydrogenases: homoisocitrate dehydrogenase from *Saccharomyces cerevisiae* (sc_HICDH), 3-isopropylmalate dehydrogenases from *Thiobacillus ferrooxidans* (tf_IPMDH), *Salmonella typhimurium* (st_IPMDH) and *Thermus thermophilus* (tt_IPMDH) and isocitrate dehydrogenase from *Escherichia coli* (ec_ICDH). Highly conserved residues in the nucleotide-binding domain within this family are shaded in blue and the conserved residues involved in the dimerization domain are colored pink. Conserved active-site residues are marked with red triangles and the nonconserved substrate, catalytic and metal-binding residues are labeled with red stars.

ion-dependent decarboxylating hydroxy-acid dehydrogenases (Grant, 1989). TDH is a member of this latter metal ion-dependent (*R*)-hydroxy-acid dehydrogenase family. This family has an evolutionarily distinct nucleotide-binding domain that differs from the more traditional pyridine nucleotide-linked dehydrogenases (Tipton & Beecher, 1994). TDH catalyzes the oxidation of (+)-tartrate to form oxaloglycolate and can also catalyze the oxidative decarboxylation of D-malate to produce pyruvate and CO_2 (Figs. 2*a* and 2*b*). Among the characterized members of the (*R*)-hydroxy-acid dehydrogenase family, only homoisocitrate dehydrogenase (HIcDH) is similar to TDH in its ability to be activated by K^+ (Lin *et al.*, 2008). However, HIcDH has been shown to follow a random mechanism (Lin *et al.*, 2006), while TDH has an ordered kinetic mechanism (Tipton & Peisach, 1990).

A detailed kinetic investigation, including pH rate-profile and isotope-effect studies, supports an acid–base catalytic mechanism with participation of general acid catalysis in the oxidative decarboxylation of D-malate (Karsten *et al.*, 2002). The reaction in the forward direction commences with a hydride transfer from the 2-hydroxy-acid substrate to NAD followed by decarboxylation. However, the reverse hydride transfer from NADH back to the oxaloacetate (OAA) intermediate is twice as fast as the decarboxylation of OAA (Tipton, 1993). However, since the re-carboxylation of pyruvate is negligible the irreversibility of this step ensures that the reaction proceeds to the pyruvate product. Significantly, the rate constant for the dissociation of the OAA intermediate from the enzyme active site is much slower than that for the dissociation of oxaloglycolate, the product of the enzyme-catalyzed oxidation of (+)-tartrate. TDH also catalyzes a third type of reaction, the decarboxylation of *meso*-tartrate to produce D-glycerate and CO_2 (Fig. 2*c*). This reaction differs from the previously described reactions in that it is formally a decarboxylation with no net oxidation or reduction; however, NAD is still required for the reaction to proceed. TDH requires both a divalent metal ion (Mn^{2+} or Mg^{2+}) and a monovalent (K^+) cation for activity. The cations have been proposed to function in substrate binding and in facilitating the decarboxylation of β-keto-acid intermediates (Karsten & Cook, 2006). Binding studies suggest a half-of-the-sites mechanism for TDH in which NAD binds to the enzyme–metal ion complexes with a stoichiometry of two per enzyme dimer (Karsten & Cook, 2006).

Previous studies have shown that each of the different substrates of TDH undergoes the same initial oxidation to produce the corresponding α-keto acid with concomitant reduction of NAD (Tipton & Peisach, 1990). The ultimate fate of these intermediates, oxaloacetate, oxaloglycolate and hydroxypyruvate (Fig. 2), seems to depend on their relative rates of dissociation from the enzyme. The oxaloglycolate obtained from the oxidation of (+)-tartrate is released and then rearranges non-enzymatically to yield dihydroxyfumarate. The failure of TDH to catalyze the decarboxylation of oxaloglycolate may simply be a consequence of unfavorable kinetics caused by the more rapid dissociation of this product (Tipton, 1993). The keto acids obtained from D-malate and *meso*-tartrate each undergo enzyme-catalyzed decarboxylation with assistance from the bound divalent metal ion, yielding pyruvate and the enol form of hydroxypyruvate, respectively. Pyruvate is released from the enzyme, while hydroxypyruvate remains bound and is subsequently reduced to D-glycerate before being released (Tipton & Peisach, 1990). Oxalate acts as a time-dependent inhibitor of TDH through the formation of an abortive enzyme–NADH–oxalate complex (Beecher *et al.*, 1994). Oxalate resembles the intermediates formed during the catalytic cycle of the enzyme because of its sp^2-hybridized C atoms and also because of its ability to form a bidentate coordinate with the active-site divalent metal ion.

TDH is an ideal system for the study of catalytic evolution since its catalytic capabilities have not been optimized for a single substrate. Our interest in this enzyme comes not only from the unusual multiple reactions that it catalyzes but also from some interesting protein-engineering challenges. For the reaction in the reverse direction, TDH produces a chiral center adjacent to another chiral carbon (Fig. 2*a*). If the specificity of this enzyme can be

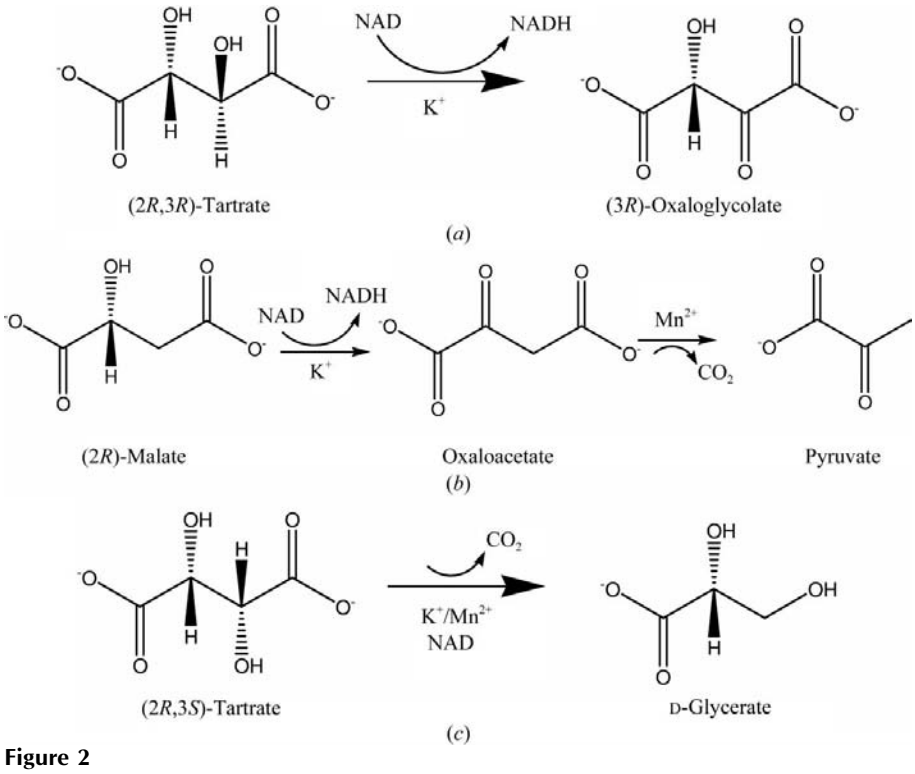

Figure 2
Reactions catalyzed by tartrate dehydrogenase. (*a*) Oxidation of (+)-tartrate. (*b*) Oxidative decarboxylation of D-malate to pyruvate. (*c*) Decarboxylation of *meso*-tartrate with net oxidation.

expanded to include nonsymmetric substrates, then a series of chiral synthons can be produced with controlled stereochemistry at adjacent C atoms. Since the final outcome of the TDH-catalyzed reactions appears to be dictated by the kinetics of the intermediate released from the active site, the structural characterization of an intermediate complex can provide valuable insights into the reasons behind the diverse consequences of these reactions.

No three-dimensional structure has been determined for TDH from any species. Here, we present the structure of a *P. putida* tartrate dehydrogenase complex containing the reduced cofactor NADH, a divalent metal ion and the intermediate analog oxalate. The interpretation of this structure provides new insights into the catalytic mechanism of this unusual enzyme and sets the stage for planned protein-engineering studies.

2. Materials and methods

2.1. Materials

All buffers, reagents and substrates were purchased from Sigma–Aldrich, the cell lines for protein expression were obtained from Invitrogen and the chromatography media were from GE Healthcare. The crystallization screens used to identify starting conditions for crystal growth were purchased from Hampton and NeXtal.

2.2. Expression and purification

The pET3a vector containing the *tdh* gene was used to transform Rosetta (DE3) *E. coli* cells (Novagen) for enzyme expression. Cells were grown at 310 K in full baffled shaker flasks and 1 m*M* isopropyl β-D-1-thiogalactopyranoside (IPTG) was used to induce expression when the OD_{600} reached 0.6. The cells were allowed to grow for an additional 8 h at 301 K after induction. The cell paste obtained was resuspended in 25 m*M* MES pH 5.8, 1 m*M* DTT, 10 m*M* KCl containing a protease-inhibitor cocktail [4-(2-aminoethyl)-benzenesulfonyl fluoride, pepstatin A, E-64, bestatin, leupeptin and aprotinin] and the supernatant was loaded onto an anion-exchange column (Q Sepharose XL). The heat step used in previously published protocols (Tipton & Beecher, 1994) was avoided since it resulted in nonhomogeneous protein, based on dynamic light scattering (DLS; Wyatt Technologies), which gave inconsistent results during crystallization trials. The protein eluted from the anion-exchange column with a salt (KCl) gradient was loaded onto a higher resolution ion-exchange column (Source 30Q). The final purification step used a gel-filtration column (Superdex 200) in a buffer consisting of 50 m*M* HEPES pH 7.5, 25 m*M* $MgSO_4$, 5 m*M* DTT and 10 m*M* KCl. Dynamic light scattering (DLS, Wyatt Technologies) was used to check the polydispersity of the protein. The overall yield was 45 mg of highly pure enzyme from 4 g of cell paste. The enzyme was concentrated to a final concentration of 60 mg ml^{-1} using a 10 000 molecular-weight cutoff Amicon concentrator before setting up crystal screens. The selenomethionine (SeMet) form of the protein was produced by the methionine-inhibition pathway method (Doublié, 1997). Intact mass spectrometry (Ohio State University Mass Spectrometry Facility) was used to confirm the incorporation of selenomethionine into the protein. Both SeMet and native enzyme were purified in a similar fashion, with the exception that a higher concentration of reducing agent was used in the SeMet protein buffer to minimize oxidation of the more sensitive selenomethionines. The resultant protein was shown to be >99% pure based on an SDS gel profile and had less than 15% polydispersity at 293 K based on DLS studies. The activity of *P. putida* TDH was measured by monitoring the production of NADH at 340 nm using D-malate as the substrate.

2.3. Crystallization of an intermediate-analog complex of TDH

Initial crystallization screening was carried out with commercial screening kits (NeXtal), but the preliminary crystals obtained from several conditions from the PACT and $AmSO_4$ suites did not diffract beyond 3.5 Å resolution. Crystals of SeMet-substituted TDH complexed with oxalate, NADH and Mg^{2+} were optimized at 293 K from new starting conditions using the hanging-drop vapor-diffusion method. The optimum crystals formed in a drop consisting of 2 µl protein solution (15 mg ml^{-1} in 50 m*M* HEPES pH 7.5, 25 m*M* $MgSO_4$, 20 m*M* DTT, 10 m*M* KCl, 5 m*M* oxalate and 5 m*M* NADH) and 2 µl reservoir solution consisting of 1.75 *M* ammonium sulfate, 0.2 *M* potassium acetate and 20 m*M* DTT. Crystals of about 0.3 × 0.2 × 0.2 mm grew within 4–5 d. The crystals were flash-frozen in liquid nitrogen following equilibration in a stabilization solution containing 2.2 *M* Li_2SO_4, 2.5 m*M* oxalate, 2.5 m*M* NADH, 5 m*M* DTT, 0.05 *M* potassium acetate, 38 m*M* HEPES pH 7.5, 19 m*M* $MgSO_4$ and 7.5 m*M* KCl. These crystals had tetragonal symmetry and the data best fitted space group $P4_32_12$, with unit-cell parameters $a = 117.27$, $b = 117.27$, $c = 291.32$ Å, $\alpha = \beta = \gamma = 90^\circ$ and a dimer of dimers in the asymmetric unit.

2.4. Data collection and processing

Initial screening of crystals flash-cooled in liquid nitrogen were carried out at 100 K using a Rigaku FR-E high-brilliance X-ray diffractometer equipped with a Saturn 92 CCD detector (Ohio Macromolecular Crystallography Consortium, The University of Toledo, USA). The complete diffraction data for the SeMet crystals were collected on Southeast Regional Collaborative Access team (SER-CAT) beamline 22-ID at the Advanced Photon Source. The Se absorption edge was identified by an X-ray fluorescence energy scan, from which the SAD data-collection experiment was designed. All data sets were indexed, integrated and scaled with *HKL*-2000 (Otwinowski & Minor, 1997). Data-collection statistics for the TDH intermediate-analog complex are reported in Table 1.

2.5. Structure determination and refinement

Experimental phases were initially obtained by inputting a 2.45 Å data set obtained from SeMet-substituted TDH into

the *SGXPro* suite (Fu *et al.*, 2005), which was able to build over 1300 amino acids into the electron-density maps of the dimer of dimers at the final stage. A higher resolution data set was collected from a different crystal and *SHARP* (de La Fortelle & Bricogne, 1997) was used to find a solution. The maps obtained from this higher resolution data set were used as a guide to build the entire molecule. Manual correction of the model into the experimental electron-density map was performed by real-space refinement with *Coot* (Emsley & Cowtan, 2004). The structure was refined by rigid-body refinement followed by restrained refinement using the program *REFMAC*5 (Murshudov *et al.*, 1997). Finally, TLS refinement (Winn *et al.*, 2001) was performed by subdividing the monomer into three subdomains (amino acids 5–158, 159–295 and 296–363), with each monomer being refined individually.

The phasing and final refinement statistics for the intermediate-analog complex are presented in Table 1.

2.6. Site-directed mutagenesis and kinetic studies

A QuickChange site-directed mutagenesis kit (Stratagene) was used to make point mutations of the proposed important active-site residues and each mutation was confirmed by nucleotide sequencing (MWG Biotech). The mutants were overexpressed in Rosetta (DE3) *E. coli* cells following induction with 1 m*M* IPTG and the cells were grown at 301 K after induction. Because of the inherent instability of some of these mutants, a reduction in growth temperature to 298 K after induction was important to avoid expression of the mutants as inclusion bodies. The mutants were each purified using a similar protocol as employed for the native enzyme. SDS–PAGE electrophoresis was used to confirm the presence of mutants which showed minimal catalytic activity.

Enzyme activity was measured in a SpectraMax 190 microplate reader at 298 K using a 96-well flat-bottom plate (Fischer Scientific) in a final volume of 200 µl. All the reactions were carried out in 100 m*M* HEPES pH 8.0. Enzymatic assays to determine kinetic parameters were carried out by varying one substrate with the other substrates held constant at saturating levels (>10 × K_m). Initial velocities were fitted to the hyperbolic curve using an enzyme-kinetics package (Keng & Viola, 1996) adapted from previous kinetics programs (Cleland, 1967).

3. Results and discussion

3.1. Overall structure of tartrate dehydrogenase

The highest quality crystals were obtained for a complex of SeMet-substituted TDH containing NADH, Mg^{2+} and the intermediate analog oxalate. Higher levels of DTT (20 m*M*) were included in the crystallization conditions to minimize the oxidation of the more sensitive selenomethionines. The presence of this antioxidant played a critical role in the improved crystal quality, resulting in a change from hexagonal to orthorhombic crystals. In the final structure three molecules of DTT were identified bound at different sites. The DTT in site 1 (Fig. 3) bridges between two arginine residues in one subunit and an asparagine in the adjacent subunit of the other dimer in the asymmetric unit, while the DTT in site 2 is positioned near the dimer interface and interacts with a backbone amide group from monomer *A* and a glutamine side chain in monomer *B*. The role of DTT in improving crystal quality is a consequence of its binding at these crucial interface regions within and between the dimers.

Table 1
Data-collection and refinement statistics for the intermediate-analog complex.

Values in parentheses are for the highest resolution shell.

Data collection	
Wavelength (Å)	0.9794
Space group	$P4_32_12$
Unit-cell parameters (Å, °)	$a = b = 117.3$, $c = 291.3$, $\alpha = \beta = \gamma = 90$
Resolution (Å)	35.6–2.0 (2.04–1.99)
No. of reflections	1662916
Unique reflections	136838
$I/\sigma(I)$	21.4 (4.97)
R_{merge}† (%)	11.2 (30.7)
Completeness (%)	99.0 (90.0)
Redundancy	12.2 (6.5)
Phasing	
No. of Se atoms	40
Phasing power	1.497
Figure of merit	0.422/0.125
Refinement	
No. of molecules in asymmetric unit	4
Wilson *B* factor (Å^2)	22.2
R_{work}/R_{free}‡ (%)	20.7/22.6
No. of atoms	
Protein	11365
Ligands	208
DTT	24
Waters	920
Average *B* factors (Å^2)	
Protein	20.4
Ligands	16.1
Waters	30.3
R.m.s.d. bonds (Å)	0.006
R.m.s.d. angles (°)	1.02
Ramachandran statistics (%)	
Most favored	89.3
Favored	9.5
Additionally allowed	0.7
Disallowed	0.4

† $R_{merge} = \sum_{hkl}\sum_i |I_i(hkl) - \langle I(hkl)\rangle| / \sum_{hkl}\sum_i I_i(hkl)$, where $I_i(hkl)$ is the intensity of an individual measurement and $\langle I(hkl)\rangle$ is the mean intensity of the reflection. ‡ $R_{work} = \sum_{hkl} ||F_{obs}| - |F_{calc}|| / \sum_{hkl} |F_{obs}|$, where F_{obs} and F_{calc} are the observed and calculated structure-factor amplitudes, respectively. R_{free} was calculated for a randomly selected 5% of the unique reflections that were omitted from structure refinement.

The asymmetric unit of the TDH complex with oxalate contains four molecules and the functional unit of TDH is a dimer composed of monomers with similar but not identical structures. Each monomer is organized into two domains and the conformation of these monomers is closed, in contrast to the more open structure found for the IPMDH substrate complex (Hurley & Dean, 1994), which shares a similar fold and topology with TDH. The nucleotide-binding domain of the TDH monomer contains the N- and C-terminal segments, while the dimerization domain consists of four sets of α-helices and antiparallel β-sheets (residues 117–256) from each monomer (Fig. 3). The active site is located in the cleft

between the two domains, and the substrate (or intermediate analog), cofactor and divalent metal ion are each well positioned in clear electron density in both active sites (Fig. 4). Each active site is constructed from residues derived from both subunits, thus establishing the dimer as the minimal functional unit. The first three residues of the N-terminus and the final C-terminal residue are disordered in the crystals and their positions were not determined in the final structure. A *MolProbity* Ramachandran analysis shows that 99.9% of the residues are found in the allowed regions of the plot, with the one exception being Gln315. This residue is found in the disallowed region in all four monomers of the asymmetric unit, with backbone dihedral angles of $\varphi = 57.9^\circ$ and $\psi = -88.0^\circ$. This residue is part of a short loop of three residues connecting two α-helices. The side-chain carbonyl of Gln makes a long hydrogen-bond contact with the side-chain guanido N atom of Arg275 and this interaction may provide sufficient stabilization energy to offset the energy penalty paid for backbone stereochemistry distortions.

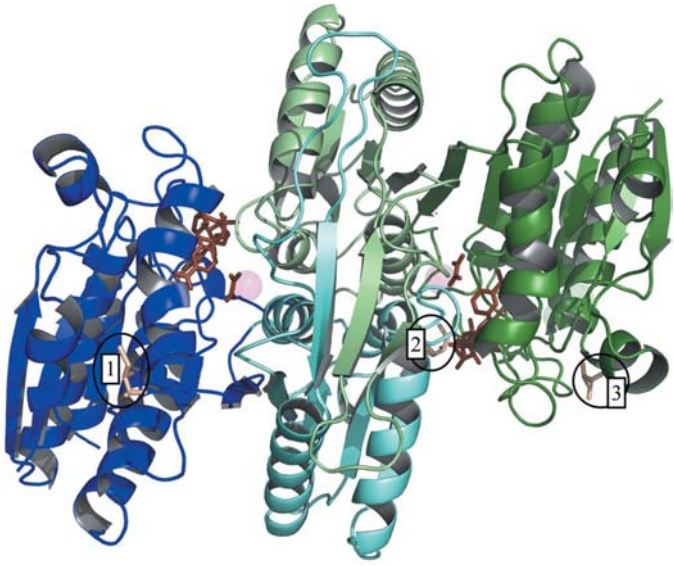

Figure 3
Overall structure of tartrate dehydrogenase. Ribbon drawing of the TDH dimer showing the domain organization and the position of the cofactor and intermediate analog (brown sticks) and the divalent metal ion (pink spheres) bound at the active site in each monomer. The two monomers are colored green and blue, with the nucleotide-binding domains shaded darker and the dimerization domains in lighter shading. Bound DTT molecules are marked in light brown, with the three binding sites numbered and circled.

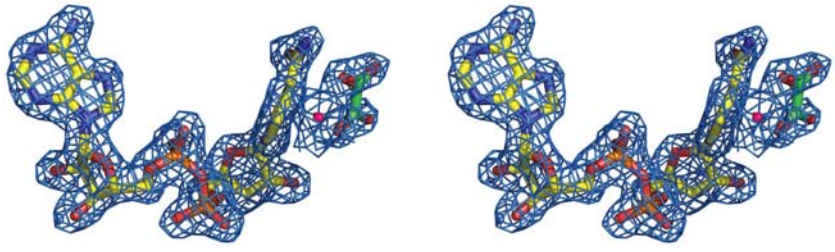

Figure 4
Simulated-annealing $F_o - F_c$ electron-density map of the active site contoured at 2.5σ, showing Mg^{2+} ion (pink sphere), oxalate ion (green sticks) and NADH (yellow sticks) modeled into the density in monomer *A*.

3.2. Structural comparison with (*R*)-hydroxy-acid dehydrogenases

Homoisocitrate dehydrogenase (HIcDH), 3-isopropylmalate dehydrogenase (IPMDH) and isocitrate dehydrogenase (ICDH) are the other structurally characterized members of the (*R*)-hydroxy-acid dehydrogenase family, with structures of the apo form of HIcDH (Miyazaki *et al.*, 2009) and several structures of IPMDHs (Wallon *et al.*, 1997) and ICDHs (Ceccarelli *et al.*, 2002; Cherbavaz *et al.*, 2000; Hurley *et al.*, 1991; Karlstrom *et al.*, 2005; Stoddard *et al.*, 1993; Xu *et al.*, 2004) having been determined from different species. The IPMDH and ICDH structures depict the state of the enzyme in the presence of substrate and a metal ion or a cofactor. Because TDH shares the highest sequence homology with IPMDH from *Thermus thermophilus* (Fig. 1), the structures and domain organizations of these related hydroxy-acid dehydrogenases were compared and found to be quite similar (Fig. 5). However, despite the overall structural similarity, significant differences are observed in several regions connecting the core secondary structure, as well as in the relative positioning of critical loops, helices and sheets. After optimization of the structural alignment, a loop and helix (residues 80–90) in TDH were found to be rotated and shifted inwards in comparison to the related region in the complex structures of IPMDH (Fig. 5). Importantly, this region participates in stabilizing the active-site architecture of IPMDH, with several residues interacting directly with the isopropyl group of the substrate (Fig. 6) as well as with the cofactor. In the IPMDH structure Asp87 forms a hydrogen bond to the nicotinamide ribose, while the residue at the corresponding position in TDH (Leu90) cannot form this interaction. Instead, this cofactor-stabilization role is now played by the adjacent Asp86 in TDH (replacing a lysine at this position in IPMDH) and the loop carrying this residue shifts inwards to support cofactor binding (Fig. 5, inset).

A second important structural difference involves the intersubunit antiparallel β-sheet located between the two domains of the enzyme, which is dramatically shifted inwards by as much as 10 Å in comparison to any of the IPMDH structures (Fig. 5). As a consequence of this shift, the closed conformation of the dimer is further stabilized upon binding of the intermediate analog (or substrate).

A comparison of the TDH structure with that of ICDH from *E. coli* confirms that it has the same overall fold and domain organization, but also identifies some additional structural variations. The intersubunit antiparallel β-sheet (Fig. 5) that is present in both IPMDH and TDH is replaced by an α-helix at the same position in bacterial ICDH. Also, part of the substrate-binding helix in TDH has been replaced by a β-sheet in the ICDH structure,

leading to replacement of the hydrophobic side chain of Leu90 with Ser113 in ICDH. Ser113 interacts with the C3 carboxyl group of isocitrate (Fig. 6), and phosphorylation of Ser113 in ICDH causes inactivation of the enzyme (Hurley *et al.*, 1989) and prevents substrate binding. Because the TDH substrates do not contain this interior carboxylate group, the presence of this serine is not required for substrate binding.

Thus, the positioning of this common loop adjacent to this substrate-binding helix is divergent in all three enzymes. This loop is dramatically shifted inwards in the TDH ternary complex to support the cofactor binding *via* Asp86, in contrast to its position in the ICDH ternary complex and the IPMDH cofactor or substrate complexes. There are also other structural features which are similar in ICDH and IPMDH but differ in this TDH structure. There is an additional loop (residue 313–319) on the outer surface of TDH which is absent in the other members of the family. In contrast, extra loops are present in the C-terminal region in IPMDH (residues 334–339) and ICDH (394–400) which are absent in TDH. Despite these structural differences between these members of the hydroxy-acid dehydrogenases, many of the active-site residues are fully conserved.

3.3. Binding of an intermediate analog

The intermediate analog oxalate (Fig. 6) is well positioned in both of the active sites of TDH through electrostatic interactions with several conserved active-site arginines. The C1 carboxylate of oxalate interacts with Arg134, which is located 2.8–2.9 Å from one of the O atoms, and there is also a complementary bidentate interaction between the C1 carboxyl O atoms and the terminal guanidinium N atoms of Arg108 at a distance of 2.9–3.2 Å (Fig. 7). An additional electrostatic interaction with the nearby Arg98 further anchors the position of this C1 carboxylate in the active site of each monomer. Arg98 is also located in close proximity to the amide N atom of the nicotinamide moiety of NAD and forms an interaction through a water-mediated hydrogen bond, thereby bridging between the substrate-binding and cofactor-binding sites. Not surprisingly, the replacement of this critical arginine at position 98 with a hydrophobic leucine causes a decrease in the stability of TDH, driving its expression into inclusion bodies that cannot be properly refolded. A more subtle change to a glutamine at this position allows the mutant protein to retain a native structure and bind its substrates with K_m values that are comparable to those of the native enzyme (Table 2). However, the catalytic efficiency of this R98Q mutant is less than 3% that of the native enzyme. These studies support a critical role for Arg98 both in the stabilization of the structural integrity of the enzyme and in orienting the substrate for optimal catalytic activity. When the other substrate-binding group Arg108 is mutated to a leucine the protein structure is also destabilized, but has been expressed in an active form at a lower temperature. The K_m value for D-malate increases by a factor of two and that for NAD by a factor of ten in this active-site mutant, leading to a decrease of over two orders of magnitude in k_{cat}/K_m for the R108L mutant (Table 2). Changing the group at position 108 to a glutamine leads to some recovery of catalytic efficiency, with a sixfold increase in k_{cat} and a 13-fold increase in k_{cat}/K_m relative to the leucine mutant. As with Arg98, this Arg108 residue is also involved in a water-mediated hydrogen bond to the nicotinamide ring of the cofactor. Basic and hydrophilic residues, including His223, Asn194 and Lys192 from the adjacent subunit, surround one face of the C4 carboxylate binding pocket and are well positioned to support substrate binding and catalysis. The other face of this binding pocket is covered by an array of hydrophobic residues, particularly Leu90 and Trp91, that shield the active site from solvent (Fig. 8).

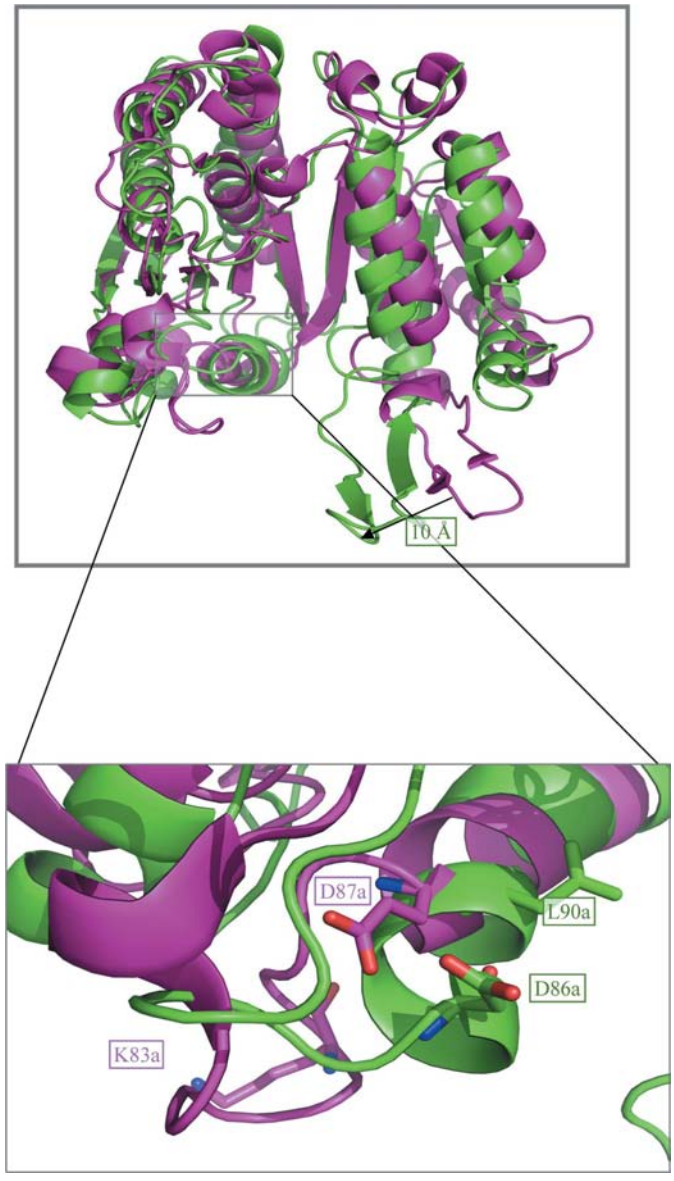

Figure 5
Structural comparison of TDH and its closest homolog by overlaying the structures of *P. putida* TDH (green) and *T. thermophilus* IPMDH (pink). Despite the similar overall fold, there are substantial shifts in a number of important secondary-structural elements. Inset: substrate-binding helix showing the position of the cofactor-binding groups Asp87 in IPMDH (in place of Leu90 in TDH) and Asp86 in TDH (in place of Lys83 in IPMDH).

Table 2
Substrate-binding mutants of tartrate dehydrogenase.

Enzyme form	k_{cat} (min^{-1})	k_{cat} (%)	K_{malate} (μM)	k_{cat}/K_{malate} (M^{-1} s^{-1})	K_{NAD} (μM)	k_{cat}/K_{NAD} (M^{-1} s^{-1})
Native	390 ± 4	100	79 ± 3	8.2×10^4	25.0 ± 0.4	2.6×10^5
R98L	−†					
R98Q	10.5 ± 0.1	2.6	98 ± 2	1.8×10^3	96 ± 2	1.8×10^3
R108L	5.2 ± 0.9	1.3	180 ± 30	4.8×10^2	240 ± 40	3.6×10^2
R108Q	34.6 ± 1.8	8.7	93 ± 18	6.2×10^3	135 ± 26	4.3×10^3

† Not expressed in stable form.

3.4. Divalent metal ion binding and its role in catalysis

Both of the carboxylate groups of the intermediate analog oxalate interact with the divalent metal ion that is required for catalysis. The divalent metal ion-binding site is hexacoordinate, with interactions with the side-chain carboxylate group of Asp250 (at 2.16 Å), equatorial and axial water molecules (2.01–2.09 Å) and the two carboxylate O atoms of the oxalate intermediate analog (2.34–2.39 Å) (Fig. 7). A carboxylate side chain (Asp225) from the adjacent subunit (2.04 Å) completes the distorted octahedral binding site. The importance of Asp250 and Asp225 as metal ion-binding ligands was verified by site-directed mutagenesis studies, which show a tenfold and 20-fold decrease in metal ion-binding affinity and a two-order-of-magnitude decrease in catalysis when either of these ligands are removed (Table 3).

3.5. Cofactor binding

NADH binds adjacent to the substrate-binding site, with the position and orientation of each structural moiety stabilized by interactions with amino-acid residues from both subunits, as well as by hydrogen-bond contacts mediated through active-site water molecules. The adenine ring of the cofactor bound in subunit *A* is positioned by a hydrogen bond between

Table 3
Metal-binding mutants of tartrate dehydrogenase.

Enzyme form	k_{cat} (min^{-1})	k_{cat} (%)	K_{Mn} (mM)
Native	390 ± 4	100	0.05 ± 0.01
D225A	0.91 ± 0.15	0.2	1.0 ± 0.4
D250A	5.3 ± 0.8	1.4	0.6 ± 0.1

Asn298 and the exocyclic amine at C6 together with several hydrophobic side chains (Ile16 and Ile291; Fig. 9). The 2′- and 3′-hydroxyl groups of the adenine ribose are hydrogen bonded to the side-chain carboxyl O atoms of Asp290. The 3′-hydroxyl also interacts with the guanidinium N atom of Arg230 from subunit *B*. The phosphate attached to the adenine ribose is stabilized by a direct interaction with the backbone NH of Gly286 and a slightly longer interaction with the side-chain hydroxyl of Ser287. The other phosphate of the pyrophosphate linker is stabilized by a water-mediated hydrogen bond to Arg230 from subunit *B*. The nicotinamide ribose hydroxyl groups form hydrogen bonds to the side-chain carboxyl of Asp86 from subunit *A* and the amide of Asn194 from subunit *B*. The Glu282 carboxyl group stabilizes the orientation of the nicotinamide ring by interacting with the NH_2 group (Fig. 9). These multiple interactions contributed by functional groups from both subunits result in a well defined binding pocket that orients the cofactor for efficient hydride transfer.

Interestingly, the orientation of the nicotinamide ring of NADH in the intermediate-analog complex of TDH is positioned in clearly defined electron density (Fig. 4). This is in contrast to the absence of well ordered density for the nicotinamide of NAD bound to its closest homolog IPMDH (Hurley & Dean, 1994). In the absence of bound substrate two possible orientations have been proposed for the cofactor in IPMDH, neither of which are the same as that observed in TDH. The residues involved in stabilizing cofactor binding in IPMDH are similar to those found in TDH, with two major

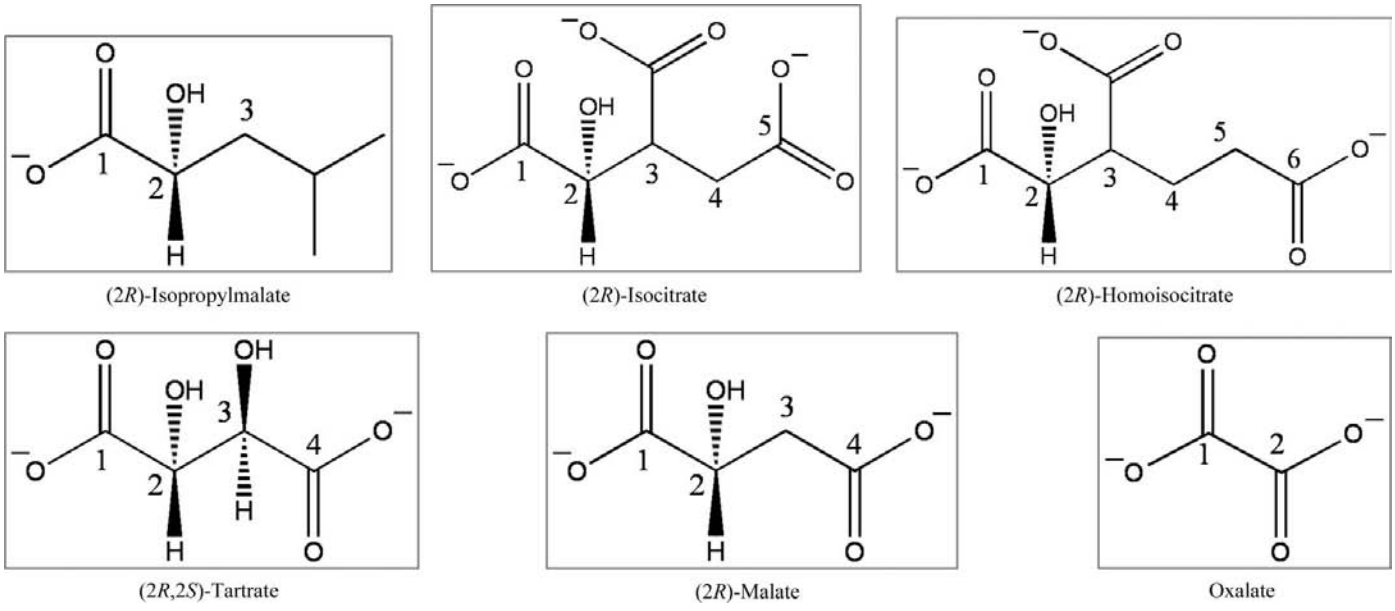

Figure 6
Comparison of the substrates of IPMDH, ICDH and HIcDH with the substrates and intermediate analog of TDH.

exceptions. The additional bonding interactions from the adjacent subunit that contribute to the binding of NADH in TDH are not present in IPMDH. The arginine from the adjacent subunit (Arg230) that interacts with the adenine ribose in TDH is replaced by a carboxyl group from Asp278 in the same subunit which plays this role in IPMDH. Hence, in the absence of the intermediate analog there are fewer interactions to stabilize cofactor binding and orient the nicotinamide ring for efficient hydride transfer in IPMDH.

3.6. The monovalent cation and its role in cofactor binding

The presence of a monovalent potassium ion is essential for the catalytic activity of TDH (Kohn *et al.*, 1968) and monovalent ions such as potassium, ammonium and rubidium were found to activate the related enzyme HIcDH (Lin *et al.*, 2008). However, the location of this monovalent cation and its exact role in the reaction has not been determined. On the basis of pH rate-profile studies the monovalent activator was proposed to bind to an ionized carboxyl side chain in HIcDH and to function to increase the affinity of the enzyme for its cofactor through interactions with the pyrophosphate moiety of NAD (Lin *et al.*, 2008). Initial velocity studies established the K_a for K^+ binding to apo TDH as 30 m*M* and this value decreased to 4 m*M* in the presence of saturating NAD (Karsten & Cook, 2006). However, potassium ions are not found in the active site in either TDH complex structure, despite the inclusion of millimolar levels of KCl in the crystallization buffers. Ammonium ions have previously also been shown to function as an activator of TDH (Kohn *et al.*, 1968) and the highly solvent-exposed active site could allow facile exchange of K^+ ions with the molar concentration of NH_4^+ ions that were used as a crystallization precipitant. Upon careful examination, one NH_4^+ ion was located within the active site in close proximity to the nicotinamide ring. This ion was identified by its high coordination number and nearly tetrahedral bonding angle (111.6°; ideal 109.5°), as well as its tendency to only coordinate to electronegative groups. This is likely to represent the monovalent cation activator site in TDH. The monovalent ion is coordinated by the backbone carbonyl groups of Pro283, His285 and Gly76, along with a side-chain carboxyl group of Glu282 (Fig. 9), thus confirming the proposed role of a carboxyl group in monovalent cation binding. However, the interaction of ammonium ions with the cofactor in TDH is through the amide O atom of the nicotinamide rather than the pyrophosphate moiety (Lin *et al.*, 2008).

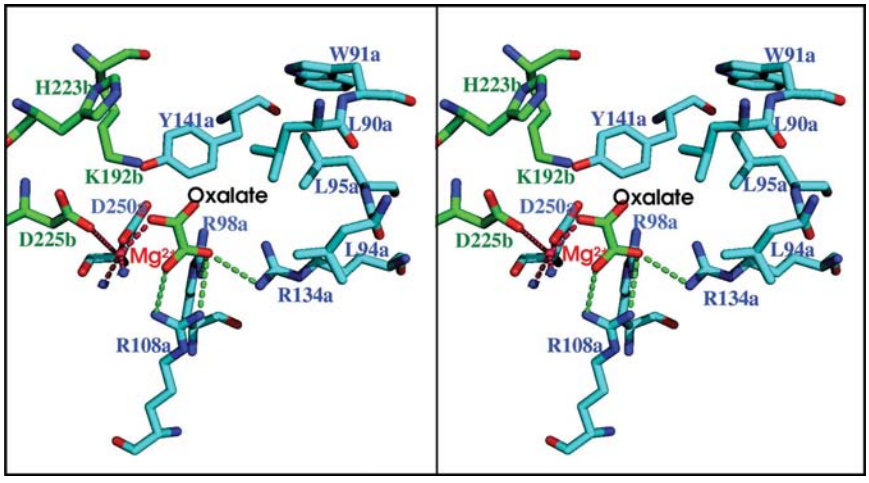

Figure 7
Stereoview of the divalent metal-ion-binding and substrate-binding sites in monomer *A*. The residues from monomer *A* are shown as blue sticks and and labeled in blue, while those from monomer *B* are shown as green sticks and labeled in green. Mg^{2+} (pink sphere) is coordinated by six ligands: two aspartate residues, two water molecules (blue spheres) and a bidentate interaction with carboxylate groups of oxalate, with the oxalate further positioned through interactions with several active-site arginines.

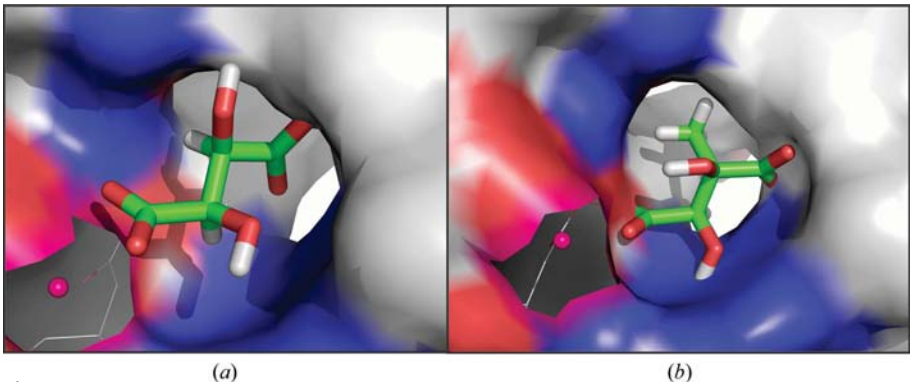

Figure 8
Space-filling model showing the charge distribution around the active-site cavity. (*a*) *meso*-Tartrate is modeled into a surface representation of the substrate-binding pocket. The surface located to the right of the bound substrate is predominately hydrophobic (white), while the surface above and below that interacts with the substrate carboxyl and hydroxyl groups is positively charged (blue). The negatively charged surface (red) to the left of the substrate provides the binding site for the divalent metal ion (pink sphere). (*b*) (2*R*,3*S*)-3-Methyltartrate is modeled into the active site with a similar orientation to that of *meso*-tartrate. The methyl group is oriented back into the hydrophobic pocket, causing the carboxylate to rotate into the plane of the C2–C3 bond and not be in position for subsequent decarboxylation.

3.7. Subunit communications and alternating-site reaction mechanism

Based upon isothermal titration calorimetry (ITC) studies, which found a sevenfold difference in NAD-binding affinity to each subunit in the dimer (Karsten & Cook, 2006), TDH has been proposed to use a 'half-of-sites' reaction mechanism to catalyze product formation. Each enzyme form was crystallized in the presence of saturating levels of NADH and a molecule of cofactor is

bound in each active site with no evidence for asymmetry in binding. However, there are numerous routes by which the binding of substrates and the release of products in one subunit can be communicated to the adjacent subunit. Five residues that originate from the other subunit are involved in substrate, cofactor and divalent metal-ion binding in the adjacent subunit of the dimer (Figs. 7 and 9). In addition, His223 from one subunit interacts with Asp86, a residue involved in cofactor binding from the opposite subunit. In a similar manner, Arg230 from the adjacent subunit provides binding interactions to the ribose and phosphate groups of the NAD cofactor (Fig. 9). Asp250, a metal-binding residue, is engaged in a monodentate interaction with Lys192 from the other subunit and Asp225 from the adjacent subunit completes the metal-ion coordination sphere (Fig. 7). There are also a number of electrostatic and hydrogen-bonding interactions across the subunit interface that serve to maintain the structural integrity of the functional dimer. From this ensemble of interactions each active site could relay information to the other subunit *via* a number of different pathways, and structural comparisons of complexes with only a single substrate or cofactor bound to the dimer will be required to narrow these possibilities.

3.8. Substrate specificity

Sequence alignments among the hydroxy-acid dehydrogenases and structural studies of ICDH and IPMDH indicate a high degree of conservation for the residues that interact with the C1 carboxylate group (Fig. 6) of their respective substrates. However, the residues that interact with the functional group at the C4 position differ within this enzyme family, providing the necessary substrate specificity for each enzyme. For TDH the binding pocket that interacts with these diverse substrate groups is formed by an array of both hydrophilic and hydrophobic residues. The hydrophilic side chain of Asn194 that interacts with the ribose ring of the cofactor is also in position to hydrogen bond to the carboxyl functional group at the C4 position of the TDH substrates (Fig. 6) through an intervening water molecule. A comparison of the active sites of TDH and IPMDH reveals that the amino-acid side chains surrounding this region of the substrate are shifted inwards in comparison to their conserved counterparts that stabilize the C1 position in IPMDH.

Several models have been proposed to account for the conformational selectivity of substrate binding that can either promote or disfavor the decarboxylation of different substrates. However, a detailed understanding of the unusual catalytic diversity of TDH has been hindered by the absence of structural information to examine these proposed binding models. An examination of the possible substrate conformers suggested a model in which bidentate metal-ion coordination to the adjacent hydroxyl groups would orient the substrate carboxyl groups to account for the products observed (Serfozo & Tipton, 1995). However, there was no direct evidence available to show metal-ion coordination to the enzyme-bound substrate. While structures of TDH with its different substrates bound are not yet available, the positioning of the active-site groups in the intermediate-analog complex provides some insights into the diversity of reactions catalyzed by this enzyme. The TDH structure with the intermediate analog oxalate shows that the divalent metal ion is within coordination distance of both carboxylate groups, consistent with this metal ion-coordination model for substrate binding. However, the divalent metal ion would have to shift position in order to coordinate to the C3 hydroxyl group and play the role in substrate conformer selectivity that has been proposed (Serfozo & Tipton, 1995).

Based on results with several malate analogs, an alternative model was proposed in which a putative hydrophobic binding pocket could provide the necessary conformer selectivity (Serfozo & Tipton, 1995). The active-site architecture of TDH has a predominant hydrophobic face that interacts with the carbon backbone of the substrate and a polar face that interacts with the functional groups. The residues shown above and below the substrate in Fig. 8(*a*) consist of the catalytic residues as well as the positively charged binding residues that interact with the functional groups of the substrate. The binding of *meso*-tartrate (modeled in Fig. 8*a*) places the C1 carboxyl group in the same position as the oxalate carboxyl group, with the C4 functional group making interactions with charged groups on the polar surface. This orientation places *meso*-tartrate in a favorable position for metal ion-supported decarboxylation after hydride transfer. In contrast, modeling of (2*R*,3*R*)-tartrate into this binding pocket (model not shown) requires a reorientation in order to avoid unfavorable interactions between either of the hydroxyl groups and this hydrophobic surface. It is this necessary repositioning

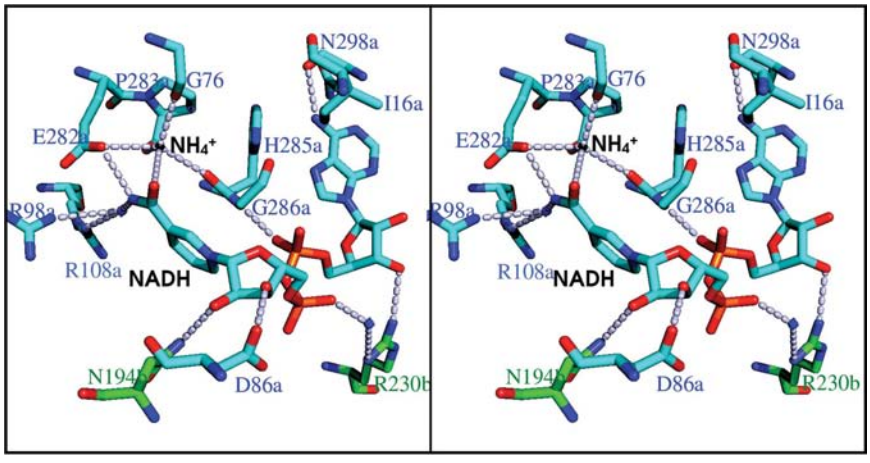

Figure 9
NAD-binding and monovalent cation-binding sites in TDH. The active-site residues from each subunit responsible for positioning the cofactor are labeled, with key water molecules indicated as blue spheres. The ammonium ion (gray sphere) is bound by interactions with backbone carbonyl O atoms and the carboxylate of Glu282 and is also within bonding distance of the amide group of the nicotinamide ring.

that presumably does not allow the decarboxylation of (+)-tartrate after TDH catalyzes its oxidation to oxaloglycolate (Fig. 2*a*).

(2*R*,3*S*)-3-Methyltartrate (equivalent to *meso*-tartrate) was found to undergo oxidation but not decarboxylation (Aktas & Cook, 2009) and this failure to decarboxylate was attributed to the accommodation of the methyl group in a hydrophobic pocket that would force the carboxylate group to become coplanar. When (2*R*,3*S*)-3-methyltartrate is modeled into the active-site cavity of the TDH structure (Fig. 8*b*) the methyl group is oriented towards a large hydrophobic cavity formed by Leu90 and Trp91, consistent with this proposal. This rotomer places the carboxylate group in the plane of the molecule and would disfavor decarboxylation.

3.9. Catalytic mechanism of tartrate dehydrogenase

The initial step in the catalytic cycle with D-malate as the substrate is a proton abstraction accompanied by hydride transfer to NAD to form the oxaloacetate intermediate (Fig. 10*a*). Lys192 is likely to be the base involved in the initial proton abstraction from the C2 hydroxyl O atom of the substrate. The ε-amino group of Lys192 must be neutral to act as a general base and the presence of a nearby protonated histidine (His223) would be sufficient to lower the pK of this functional group. This histidine is substituted by a neutral amino acid in both ICDH and IPMDH, thereby requiring some other interactions to allow this lysine to serve as a general base in these enzymes (Kim *et al.*, 2003). The lysyl amino group is likely to act *via* a proton relay through a nearby active-site water molecule which initially accepts the proton. This water molecule is positioned through hydrogen-bonding interactions with Lys192 and Asn194. Hydride transfer to the cofactor will be stabilized by the monovalent metal ion near the nicotinamide ring. Decarboxylation of the intermediate proceeds with Lewis acid assistance from the divalent metal ion to give enolpyruvate and CO_2 products

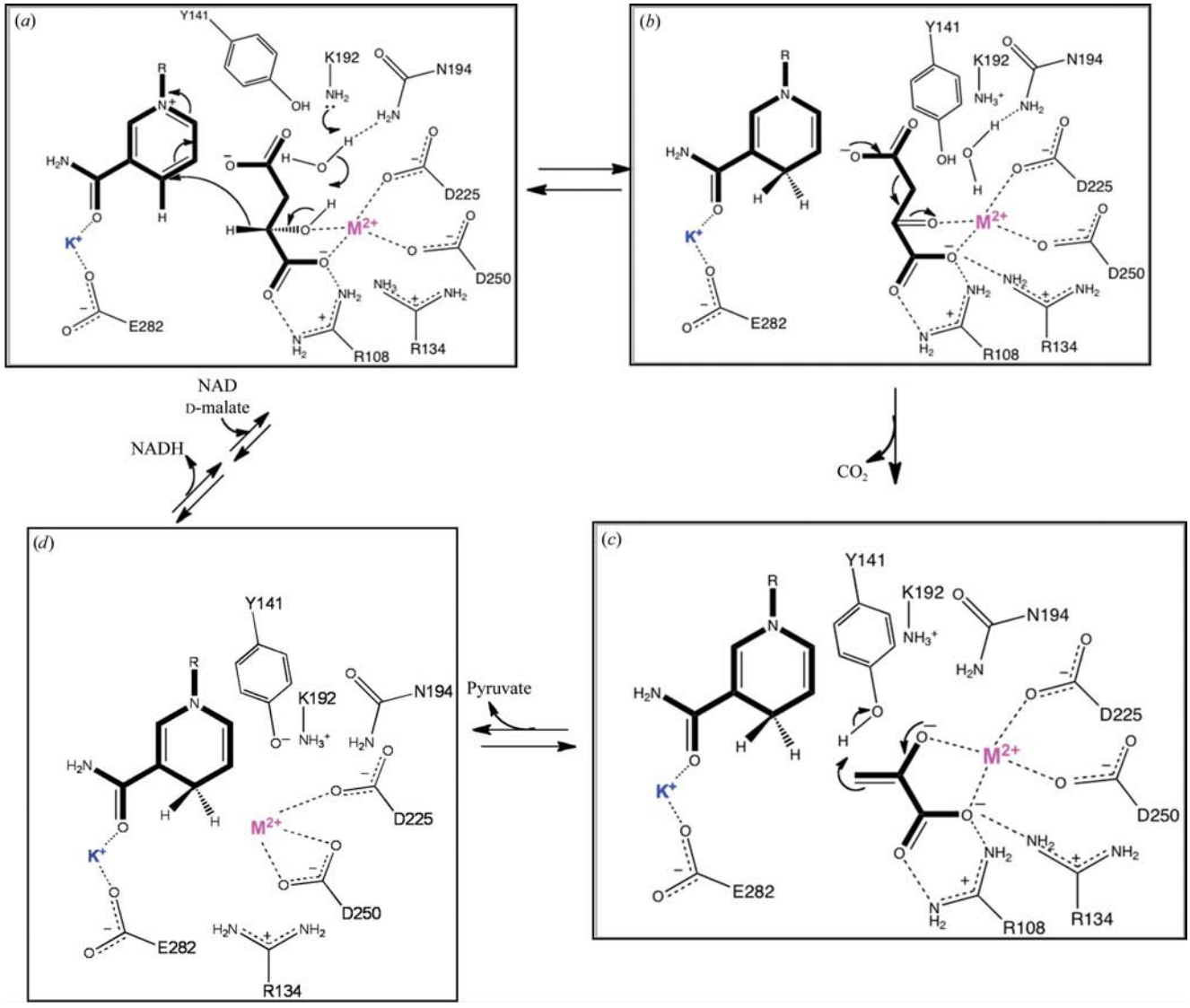

Figure 10
Proposed catalytic mechanism of TDH.

(Fig. 10*b*). Oxalate is an analog of the enolpyruvate intermediate that is formed in the TDH-catalyzed oxidative decarboxylation of D-malate, and the oxalate complex structure represents this enzyme intermediate. Dissociation of carbon dioxide and tautomerization of enolpyruvate assisted by Tyr141 acting as a general acid (Fig. 10*c*) leads to the final product. A tyrosine at the corresponding position has been proposed to play this role in the other members of the β-hydroxyacid decarboxylase family (Aktas & Cook, 2009). Dissociation of pyruvate from the enzyme leaves the NADH product complex (Fig. 10*d*) that has now been structurally characterized. Departure of the reduced cofactor and a proton transfer from Lys192 to Tyr141, followed by binding of the oxidized cofactor and substrate, completes the catalytic cycle (Fig. 10).

The authors thank Dr Paul Cook (University of Oklahoma) for providing the *tdh* gene, Dr David Coe for the initial cloning and purification of TDH while at the University of Toledo and Dr Alexander Pavlovsky (University of Toledo) for assistance with model building and refinement. Use of the Advanced Photon Source was supported by the US Department of Energy, Basic Energy Sciences, Office of Science under contract No. W-31-109-ENG-38. GM/CA-CAT has been funded in whole or in part with Federal funds from the National Cancer Institute (Y1-CO-1020) and the National Institute of General Medical Science (Y1-GM-1104). We thank the staff at beamlines GM/CA-CAT and SER-CAT for technical support during data collection.

References

Aktas, D. F. & Cook, P. F. (2009). *Biochemistry*, **48**, 3565–3577.
Beecher, B. S., Koder, R. L. & Tipton, P. A. (1994). *Arch. Biochem. Biophys.* **315**, 255–261.
Ceccarelli, C., Grodsky, N. B., Ariyaratne, N., Colman, R. F. & Bahnson, B. J. (2002). *J. Biol. Chem.* **277**, 43454–43462.
Cherbavaz, D. B., Lee, M. E., Stroud, R. M. & Koshland, D. E. (2000). *J. Mol. Biol.* **295**, 377–385.
Cleland, W. W. (1967). *Adv. Enzymol.* **29**, 1–32.
Doublié, S. (1997). *Methods Enzymol.* **276**, 523–529.
Emsley, P. & Cowtan, K. (2004). *Acta Cryst.* D**60**, 2126–2132.
Fu, Z.-Q., Rose, J. & Wang, B.-C. (2005). *Acta Cryst.* D**61**, 951–959.
Grant, G. A. (1989). *Biochem. Biophys. Res. Commun.* **165**, 1371–1374.
Hurley, J. H. & Dean, A. M. (1994). *Structure*, **2**, 1007–1016.
Hurley, J. H., Dean, A. M., Koshland, D. E. & Stroud, R. M. (1991). *Biochemistry*, **30**, 8671–8678.
Hurley, J. H., Stroud, R. M., Thorsness, P., Ramalingam, V., Helmers, N. & Koshland, D. E. (1989). *Proc. Natl Acad. Sci. USA*, **86**, 8635–8639.
Karlstrom, M., Stokke, R., Steen, I. H., Birkland, N. K. & Ladenstein, R. (2005). *J. Mol. Biol.* **345**, 559–577.
Karsten, W. E. & Cook, P. F. (2006). *Biochemistry*, **45**, 9000–9006.
Karsten, W. E., Tipton, P. A. & Cook, P. F. (2002). *Biochemistry*, **41**, 12193–12199.
Keng, Y. F. & Viola, R. E. (1996). *Arch. Biochem. Biophys.* **335**, 73–81.
Kim, T.-K., Lee, P. & Colman, R. F. (2003). *J. Biol. Chem.* **278**, 49323–49331.
Kohn, L. D., Packman, P. M., Allen, R. H. & Jakoby, W. B. (1968). *J. Biol. Chem.* **243**, 2479–2485.
La Fortelle, E. de & Bricogne, G. (1997). *Methods Enzymol.* **276**, 472–494.
Lin, Y., Alguindigue, S. S., Volkmann, J., Nicholas, K. M., West, A. H. & Cook, P. F. (2006). *Biochemistry*, **46**, 890–898.
Lin, Y., West, A. H. & Cook, P. F. (2008). *Biochemistry*, **47**, 10809–10815.
Miyazaki, J., Asada, K., Fuchinobu, S., Kuzuyama, T. & Nishiyama, M. (2009). *J. Bacteriol.* **187**, 6779–6788.
Murshudov, G. N., Vagin, A. A. & Dodson, E. J. (1997). *Acta Cryst.* D**53**, 240–255.
Otwinowski, Z. & Minor, W. (1997). *Methods Enzymol.* **276**, 307–326.
Ruszczycky, M. W. & Anderson, V. E. (2004). *Bioorg. Chem.* **32**, 51–61.
Serfozo, P. & Tipton, P. A. (1995). *Biochemistry*, **34**, 7517–7524.
Stoddard, B. L., Dean, A. & Koshland, D. E. (1993). *Biochemistry*, **32**, 9310–9316.
Tipton, P. A. (1993). *Biochemistry*, **32**, 2822–2827.
Tipton, P. A. (1996). *Biochemistry*, **35**, 3108–3114.
Tipton, P. A. (2000). *Pept. Protein Lett.* **7**, 323–332.
Tipton, P. A. & Beecher, B. S. (1994). *Arch. Biochem. Biophys.* **313**, 25–31.
Tipton, P. A. & Peisach, J. (1990). *Biochemistry*, **29**, 1749–1756.
Wallon, G., Kryger, G., Lovett, S. T., Oshima, T., Ringe, D. & Petsko, G. A. (1997). *J. Mol. Biol.* **266**, 1016–1031.
Winn, M. D., Isupov, M. N. & Murshudov, G. N. (2001). *Acta Cryst.* D**57**, 122–133.
Xu, X., Zhao, J., Xu, Z., Peng, B., Huang, Q., Arnold, E. & Ding, J. (2004). *J. Biol. Chem.* **279**, 33946–33957.